JOURNAL OF MATERIALS SCIENCE **40** (2005) 399–410

Determination of critical material parameters for numerical simulation of acrylic sheet forming

Y. DONG, R. J. T. LIN, D. BHATTACHARYYA*
Centre for Advanced Composite Materials (CACM), Department of Mechanical Engineering, University of Auckland, Private Bag 92019, Auckland, New Zealand
E-mail: d.bhattacharyya@auckland.ac.nz

In order to accurately demonstrate the material behavior during numerical simulation of thermoforming, the critical material parameters of any specific polymeric material need to be determined properly. In this study, acrylic sheets (Poly(methyl methacrylate), PMMA) of both opaque and transparent nature were chosen as the sample materials due to their widespread usage for the manufacturing of bathwares and kitchen appliances. Hyperelastic theory (e.g., Mooney-Rivlin and Ogden models) was employed with experimental verification to obtain the critical material parameters of PMMA. By conducting uniaxial tensile tests at elevated temperatures between 150 and 190°C and utilising the least square method (LSM), the major material parametric functions were derived in terms of forming temperature. Preliminary application on simulation of free inflation of a bubble profile resulted in promising agreement with the experimental data validating the developed parameters.

Nomenclature

C	Constant of curve-fitting exponential function for two-term Mooney-Rivlin model (MPa)
C_{ij}	Empirically determined constants of strain energy function ($i = 0, 1, 2 \ldots M$ and $j = 0, 1, 2 \ldots N$)
C_{10}	Two-term Mooney-Rivlin model material parameter (MPa)
C_{01}	Two-term Mooney-Rivlin model material parameter (MPa)
E	Young's modulus for infinitesimal deformation (MPa)
E'	Storage modulus (Pa)
E''	Loss modulus (Pa)
$\mathrm{F_m}(\lambda)$	Fitted model regression function in terms of the stretch ratio λ
f	Frequency (Hz)
H	Vertical distance from the apex of the inflated bubble (mm)
I_i	Strain tensor invariants in the i-th directions ($i = 1, 2, 3$)
k	Constant of curve-fitting exponential function for two-term Mooney-Rivlin model (1/°C)
l	Specimen length after thermal conditioning (mm)
l_0	Original length of the specimen in the shrinkage test (mm)
L_0	Original gauge length of acrylic specimen (mm)
L	Length after uniaxial tension (mm)
M	Constant of curve-fitting exponential function for single term Ogden model (MPa)
n	Constant of curve-fitting exponential function for single term Ogden model (1/°C)
Q	Minimum of sum of the squared deviations
R^2	R-squared value
T	Temperature (°C)
T_g	Glass transition temperature (°C)
t	Time at final configuration of the material (s)
t_0	Time in the initial state of the material (s)
W	Strain energy function
y_m	Observed scattered values
α	Single term Ogden model material parameter
α_i	Ogden model material parameter ($i = 1, 2, 3\ldots$)
β	Single term Ogden model material parameter (MPa)
β_i	Ogden model material parameter ($i = 1, 2, 3\ldots$) (MPa)
$\tan\delta$	Loss tangent ($\tan\delta = E''/E'$)
$\tan\delta_{max}$	Maximum value of loss tangent
λ	Principal stretch ratio
λ_i	Stretch ratio in the i-th directions ($i = 1, 2, 3$)
σ_{BT}	True stress of equibiaxial tension (MPa)
σ_{UT}	True stress of uniaxial tension (MPa)
σ_{11}	Cauchy stress tensor in the first principal direction (MPa)
σ_{22}	Cauchy stress tensor in the second principal direction (MPa)

*Author to whom all correspondence should be addressed.

1. Introduction

Thermoforming is considered to be a "secondary" plastic manufacturing process in which a polymeric sheet is reheated and moulded using vacuum or pressure [1]. In the thermoforming processes, the quality of the final part is greatly dependent on the material flow and the resulting thickness distribution. The traditional "trial and error" methods used for optimising these manufacturing processes, as done today, are quite time-consuming and expensive, and hence numerical simulation has been introduced as a powerful analytical tool for process optimisation to avoid the waste of resources.

For numerical simulations of thermoforming polymeric materials, hyperelastic and viscoelastic models are the two commonly used rheological models. The emphasis of current study is on the hyperelastic models due to their better suitability for materials, which are isotropic, highly elastic and incompressible under the condition of relatively high strain rate. Research has been carried out on applying both numerical and analytical models [1–7], which are based on the strain energy function. In addition, the material parameters obtained from these theoretical models are considered to be able to reflect the actual material behaviour, such as the non-linearity typically associated with large strains and large deformation, and are valid for predicting the thickness distribution in a simulation. In this study, both of the well-known Mooney-Rivlin and Ogden models are adopted as the hyperelastic models.

Previous work [5–9] has shown that the characterisation of a polymeric material, such as PMMA, at the elevated temperatures can be carried out with more sophisticated facilities; however, the classic uniaxial and equibiaxial tensile tests can also be used for similar characterisation processes [2, 10–12] to achieve the same results. Therefore in this study, uniaxial tensile tests at elevated temperatures have been used in conjunction with the least square method (LSM) to determine the critical material parameters for applying in the hyperelastic models.

This paper describes the theoretical background of the two hyperelastic models and the designed experimental programmes with the aim of determining the influences of temperature-dependent material parameters so that the finite element method (FEM) based analytical tool PAM-FORM^{TM} [13] may be fruitfully used for modelling the thermoforming processes. Furthermore, the preliminary FEM application of a bubble inflation case is used to demonstrate the validity of the obtained material parameters in the hyperelastic models.

2. Theory and constitutive relationships

2.1. Strain energy function

Generally hyperelastic models demonstrate the material strain levels that exceed the simple Hookean spring condition where stress is proportional to strain and the proportionality constant is the Young's modulus [3]. Consequently the work done by the stresses during a deformation process is dependent solely on the initial state at time t_0 and the final configuration at time t, the behaviour of the material is said to be path-independent and the material is termed as "*hyperelastic*" [14].

Hyperelastic models can be developed by constructing the form of strain energy function W for an isotropic material [10]. This function can be explicitly expressed by the sum of a series of terms involving $(I_1 - 3)$ and $(I_2 - 3)$ with the assumption of incompressibility $(I_3 = 1)$,

$$W = \sum_{i,j=0}^{M,N} C_{ij}(I_1 - 3)^i (I_2 - 3)^j \qquad (1)$$

where C_{ij} are empirically determined material parameters and I_1, I_2, I_3 are the principal strain invariants. When the material is undeformed, both W and C_{00} are zero. This equation is a general form of strain energy function, from which a significant number of hyperelastic models and theories have been developed; nevertheless each of them has its individual restriction on material selection and properties, thermoforming methods and the correlation with the experimental results [12]. The Mooney-Rivlin and Ogden models are two typical examples developed from this strain energy function.

2.2. Mooney-Rivlin model

By performing experiments on two different types of vulcanised rubber, Rivlin and Saunders [15] constructed their own strain energy function given by

$$W = C_{10}(I_1 - 3) + f(I_2 - 3) \qquad (2)$$

where the function, $f(I_2 - 3)$, was determined by experiments. It can be easily found that if $f(I_2 - 3)$ is assumed to be proportional to $(I_2 - 3)$ due to the experimental observation of direct proportionality of shear stress to the shear angle in simple shear, Rivlin and Saunders' strain energy function can be simplified as the Mooney function [16],

$$W = C_{10}(I_1 - 3) + C_{01}(I_2 - 3) \qquad (3)$$

Therefore, Equation 3 is also called Mooney-Rivlin strain energy function or Mooney-Rivlin model. Mooney's strain energy function is widely used by many theoretical investigators and analysts to solve the large elastic deformations of rubber-like materials [1, 3, 5, 17, 18].

For uniaxial tension (i.e., $\lambda_1 = \lambda, \lambda_2 = \lambda_3 = \frac{1}{\sqrt{\lambda}}$), the constitutive relation becomes

$$\sigma_{UT} = \sigma_{11} = 2C_{10}\left(\lambda^2 - \frac{1}{\lambda}\right) + 2C_{01}\left(\lambda - \frac{1}{\lambda^2}\right) \qquad (4)$$

where λ_i is the stretch ratio in i-th direction ($i = 1, 2, 3$), λ is the principal stretch ratio ($=L/L_0$, where L_0 and L denote the gauge lengths before and after the test), σ_{UT} and σ_{11} are the true stress of uniaxial tension and Cauchy Stress tensor in the first principal direction respectively. When $\lambda \to 1$, the derivative of Equation 4

can be simplified as

$$E = \lim_{\lambda \to 1} \frac{\partial \sigma_{11}}{\partial \lambda} = 6(C_{10} + C_{01}) = Ce^{-\mathrm{kT}} \qquad (5)$$

where E is Young's modulus for infinitesimal deformation, C and k are two constants obtained from the curve-fitted exponential function using LSM, and T is the forming temperature.

Similarly, the constitutive relation for equibiaxial tension (i.e., $\lambda_1 = \lambda_2 = \lambda$) can be expressed as

$$\sigma_{\mathrm{BT}} = \sigma_{11} = \sigma_{22} = 2C_{10}\left(\lambda^2 - \frac{1}{\lambda^4}\right) + 2C_{01}\left(\lambda^4 - \frac{1}{\lambda^2}\right) \qquad (6)$$

where σ_{BT} and σ_{22} are the true stress of equibiaxial tension and Cauchy Stress tensor in the second principal direction respectively.

2.3. Ogden model

Alternatively, the strain energy function defined by Ogden [19] correlated with the principal stretch ratios instead of the principal strain invariants is given by

$$W = \sum_{i=1}^{n} \frac{\beta_i}{\alpha_i}\left(\lambda_1^{\alpha_i} + \lambda_2^{\alpha_i} + \lambda_3^{\alpha_i} - 3\right) \qquad (7)$$

where α_i and β_i are experimentally determined material parameters. These two parameters can be non-integer and/or negative with only one restriction that the value of the strain energy function W in Equation 7 must always remain positive.

For uniaxial tension, the constitutive relation of Equation 7 may be shown as

$$\sigma_{\mathrm{UT}} = \sigma_{11} = \sum_{i=1}^{r} \beta_i\left[\lambda^{\alpha_i} - \lambda^{-\frac{\alpha_i}{2}}\right] \qquad (8)$$

In the special case of the single-term Ogden model (i.e., $i = 1$), when $\lambda \to 1$ [1], the derivative of Equation 8 can be simplified as

$$E = \lim_{\lambda \to 1} \frac{\partial \sigma_{11}}{\partial \lambda} = \frac{3}{2}\alpha\beta = Me^{-\mathrm{nT}} \qquad (9)$$

where M and n are again two constants obtained from the curve-fitted exponential function using LSM and T is the forming temperature. Both Equations 5 and 9 are the simplified single exponential correlations between the Young's modulus and forming temperature, because the actual curve-fitted functions are more complex containing a series of exponential terms.

The constitutive relation for equibiaxial tension can be shown as

$$\sigma_{\mathrm{BT}} = \sigma_{11} = \sigma_{22} = \sum_{i=1}^{r} \beta_i[\lambda^{\alpha_i} - \lambda^{-2\alpha_i}] \qquad (10)$$

From Equations 8 and 10, apparently a large number of material parameters are difficult to obtain empirically by doing least square curve-fitting [20]. Since the single-term Ogden formulation can depict good material characterisation without resulting in significant adverse influence on the numerical simulation of thermoforming, it has been adopted effectively as the backbone of the hyperelastic model for numerical analysis.

3. Experimental details

3.1. Materials

Acrylic (PMMA) sheets, are very suitable for thermoforming process in the plastic moulding manufacturing. Therefore, in order to understand the material behaviour of PMMA under thermoforming through experimental and numerical analyses, two types of commercially available acrylic sheets: SHINKOLITE® sanitary grade (opaque, 3 mm thick) and general-purpose grade (transparent, 2.76 mm thick) were used in this study.

3.2. Viability of characterisation tests

To ensure accurate application of material characteristics in the analytical models, Three types of tests including DMTA test, shrinkage test and hot tensile test were conducted.

The DMTA test was used to determine the glass transition temperature (T_{g}) of PMMA, below which the change from rubbery to glassy state of any particular polymer takes place [20]. Once T_{g} of the PMMA sheet was decided, the forming temperature was set 30–40°C above T_{g} [3]. In this study, T_{g}, measured by DMTA test is defined as the peak of loss tangent (tanδ) vs. temperature curve, where tan δ is ratio (E''/E') of the loss modulus E'' over the storage modulus E' [21].

The purpose of shrinkage test was to investigate whether the received PMMA sheets possessed any directional properties (anisotropy) due to the molecular orientation and the manufacturing method. It is to be noted that anisotropic material properties may greatly affect the implementation of isotropic hyperelastic materials.

Due to the rubbery material behaviour of PMMA at elevated temperatures where thermoforming was performed, hot tensile test was set up to account for not only high temperature, but also the large strain at relatively high strain rate and the viscous state of the softened acrylic material. In addition, hot tensile tests provided a reasonable set of temperature dependent data under uniaxial tension to predict PMMA material parameters in the hyperelastic models for thermoforming process simulation. Interestingly this might provide the plastic engineers a good and fast empirical methodology to replace the more complex biaxial tensile test as well as sustain the viable process simulation results.

3.3. Material characterisation and results

In DMTA test, specimens were produced with dimensions of 40 mm long $\times$10 mm wide from both materials. Thermal analyser DMTA V (Rheometric Scientific, Inc., USA) was used in the three-point bending configuration under oscillations of varied frequency (0.1–10 Hz) at the temperature range from 90 to 150°C.

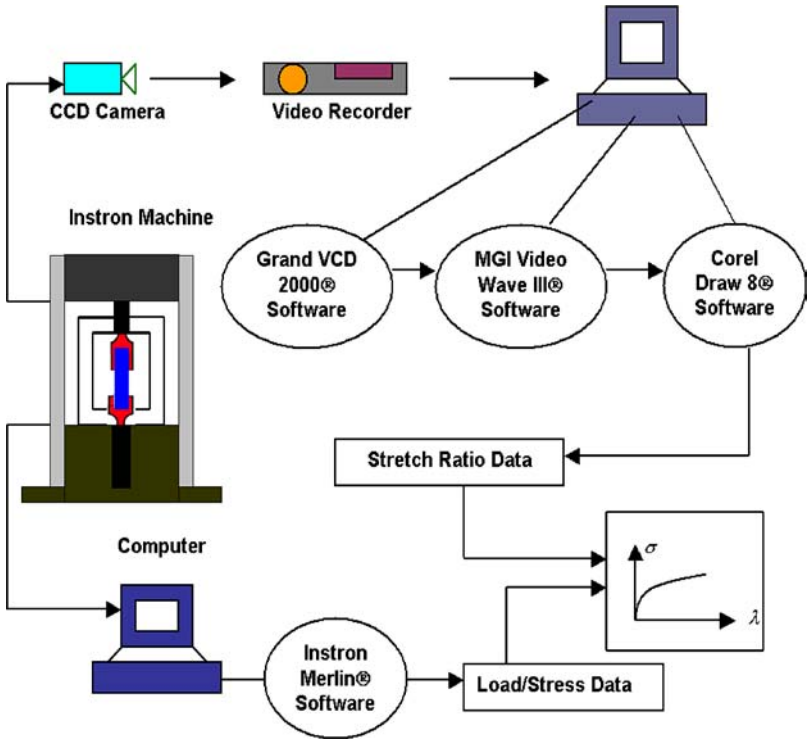

Figure 1 Schematic of data acquisition system in the hot tensile tests using the non-contact method.

The ramp rate for the DMTA test was controlled at 2°C/min by liquid nitrogen flow.

Shrinkage tests were conducted by elevating the temperature to 160, 170, 180 and 190°C, which were akin to the real forming condition in the thermoforming processes. Specimens of 110 mm × 110 mm square sheets cut from both edges and the central parts of the received acrylic sheets were prepared with four marking lines in the 0°, 45°, 90° and 135° directions. Each square sheet was heated up to the prescribed temperature and maintained at that temperature for about 30 min before being cooled down to room temperature. The length of each marked line was measured twice, once before heating and once after the heating-cooling cycle (l). The change of length measured in each direction before and after thermal conditioning was used to calculate the shrinkage (%).

Hot tensile tests were carried out using an Instron tensile testing machine incorporated with an environmental chamber. The crosshead speed was set as 250 mm/min for all the tests and desirable temperatures were from 150 to 190°C with 10°C increment. Specimens with the dimensions of 63.5 mm long × 10 mm wide were prepared with two lines etched 7 mm apart as the original gauge length in the middle portion of the test specimens. Self-tightening jaws were adopted to prevent the slippage of the specimen during the test due to the change of material state at the elevated temperature. A thermocouple was attached on the specimen to monitor the correct material temperature for test. Furthermore, for large strains at high strain rate, an ordinary extensometer was no longer suitable for measuring the deformation; therefore, video camera was used to record the material deformation process for the photographic analysis of the stress-strain variation, Fig. 1, and to calculate the stretch ratio of the specimen. After comparing the results with the computer controlled crosshead movement, reliable data of the material deformation could be obtained subsequently for establishing the stress-stretch ratio curves.

In DMTA tests, the $\tan\delta_{max}$ and the corresponding T_g values at different frequencies from 0.1 to 10 Hz are listed in Table I. Fig. 2 shows the change of loss tangent against temperature at the frequency of 1 Hz for both types of acrylic sheets. It is clear that when the temperature is raised above the glass transition temperature, the loss tangent curves exhibit a decreasing trend as the temperature increases up to about 160°C. After that the values of the loss tangent flatten out despite further increase in temperature. As the values of the loss tangent at these temperatures are well below 1, which implies that the storage modulus becomes bigger than loss modulus ($E' > E''$), the chain rotation and uncoiling for the long chain molecules of PMMA take place with a minor viscous effect, so that the rubber-like behaviour is manifested [1, 22]. It further emphasises the suitability of adopting hyperelastic models in the numerical simulation of thermoforming acrylic sheets.

TABLE I Glass Transition Temperatures of PMMA at multi-frequencies ranging from 0.1 to 10 Hz at the ramp rate 2°C/min

	Opaque		Transparent	
Frequency (f in Hz)	$\tan\delta_{max}$	T_g (°C)	$\tan\delta_{max}$	T_g (°C)
0.1	2.7334	116.88	2.1211	125.34
0.3	1.5381	120.72	1.6411	129.24
1	1.6094	124.67	1.6674	132.76
5	1.6033	130.72	1.6208	138.90
10	1.6187	134.00	1.6228	141.79

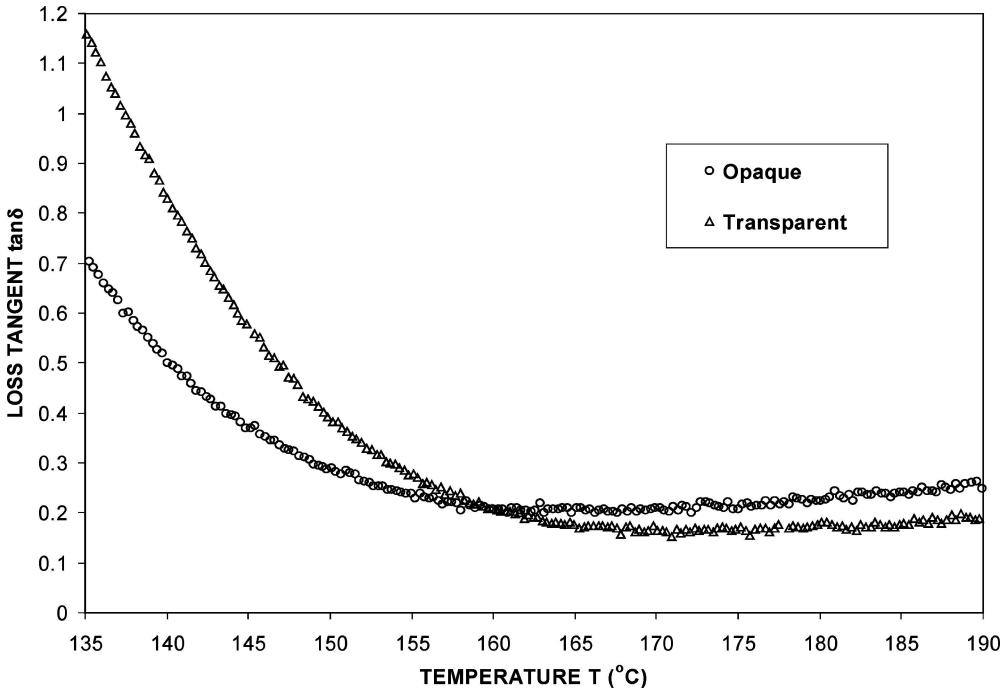

Figure 2 Typical loss tangent (tanδ) vs. temperature curves at the frequency of 1 Hz with the ramp rate of 2°C/min.

The results of shrinkage tests show that a shrinkage of 1.5 to 2.0% was observed at all test temperatures, the change of temperature level only had a minor effect on both opaque and transparent sheets and the values in different directions exhibited no dramatic discrepancy. As a consequence, these acrylic sheets have been confirmed to have the minimal orientation above their glass transition temperatures and may be treated as isotropic materials for further computer simulation using PAM-FORM™—an explicit finite element computer code based on Ogden or Mooney-Rivlin model that adopts an isotropic constitutive law.

From the hot tensile tests, the associated true stress level was calculated with each stretch ratio obtained using both photographic and crosshead movement methods, Fig. 3. Even though more precise results of stretch ratio calculation could be produced with photographic analysis, the process of analysing one specimen became much more tedious. In order to cope with the large number of specimens, the results based on the crosshead movements appeared to be accurate enough to justify their further use in this study. This observation also got support from Lai and Holt [23, 24].

For deriving the major material parametric functions, these tensile test data have been curve-fitted with a two-term Mooney-Rivlin model and a single-term Ogden model based on general non-linear LSM criterion, Equation 11.

$$Q = \min\left\{\sum_{M=1}^{N}[F_{\mathrm{m}}(\lambda) - y_{\mathrm{m}}]^2\right\} \qquad (11)$$

where Q is the minimum of sum of the squared deviations, which preferably should be as close to zero as possible; $F_{\mathrm{m}}(\lambda)$ is a fitted model regression function in terms of the stretch ratio λ and y_{m} are the observed scattered values (experimental data).

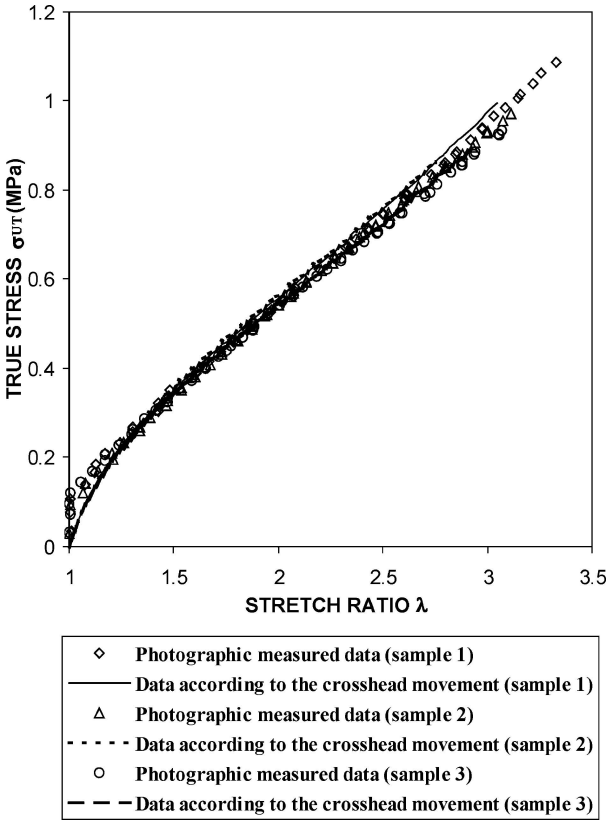

Figure 3 Comparison of true stress vs. stretch ratio data according to the crosshead movement and photographic measurement of deformation respectively for opaque acrylic sheet at 500 mm/min crosshead speed and temperature of 180°C.

A simple regression based on the "trial and error" method to achieve the optimal parameters was applied using the "Solver" tool of MS Excel® program. Material parameters in these two hyperelastic models were determined using Equations 4 and 8 with non-constraints in Mooney-Rivlin model and partially

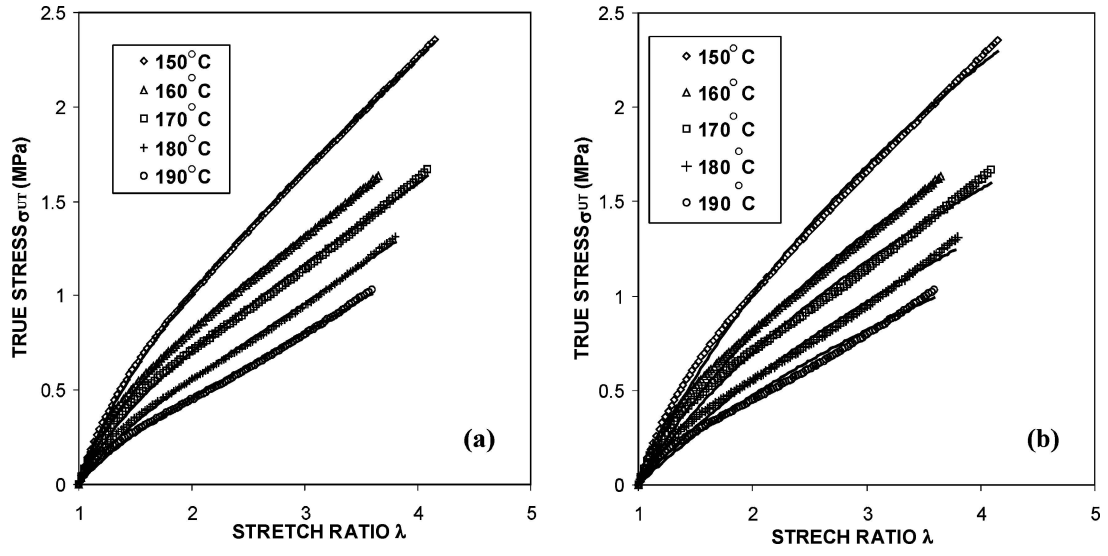

Figure 4 True stress vs. stretch ratio curves for opaque acrylic sheets at elevated temperatures from 150 to 190°C with the crosshead speed of 250 mm/min. Curve-fitting (—) with hyperelastic models using the least square method: (a) two term Mooney-Rivlin model and (b) single Ogden model.

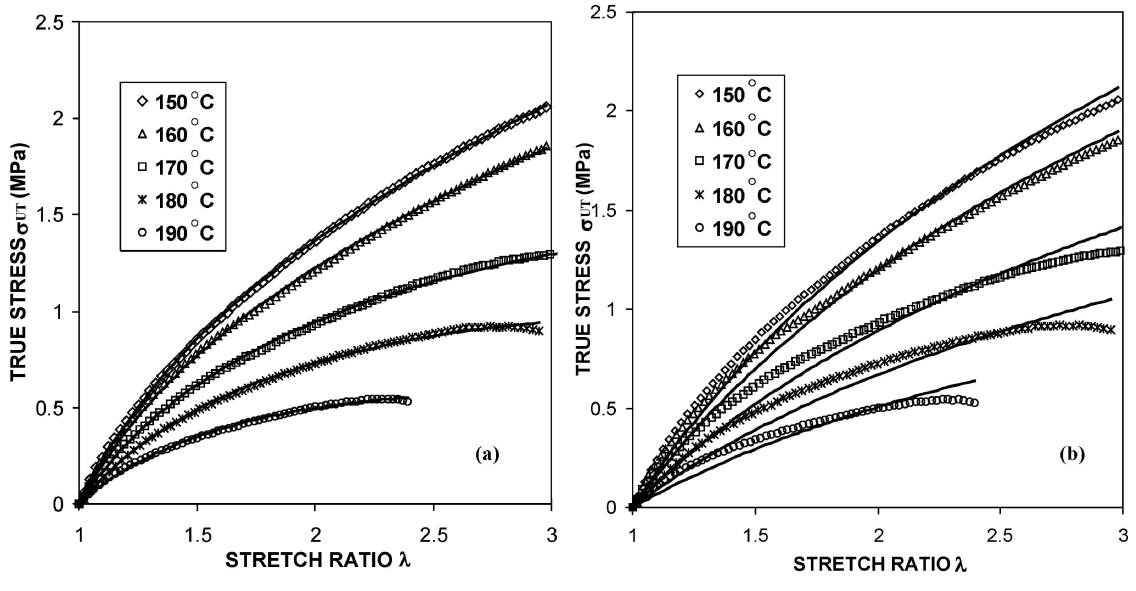

Figure 5 True stress vs. stretch ratio curves for transparent acrylic sheets at elevated temperatures from 150 to 190°C with the crosshead speed of 250 mm/min. Curve-fitting (—) with hyperelastic models using the least square method: (a) two term Mooney-Rivlin model and (b) single Ogden model.

bound constraints ($0 < \beta \leq 10$ for opaque PMMA and $0 < \beta \leq 150$ for transparent PMMA) in Ogden model. Curves of true stress vs. stretch ratio at various temperatures are shown in Figs 4 and 5. In addition, Tables II and III show the obtained material parameters of the two hyperelastic models along with the minimum values of Q and $\lim_{\lambda \to 1} \frac{d\sigma}{d\lambda}$ to validate the correlation with the experimental data.

TABLE II Mooney-Rivlin material parameters for acrylic sheets (opaque and transparent) between 150 and 190°C at the crosshead speed of 250 mm/min

Type	Temperature (°C)	C_{10} (MPa)	C_{01} (MPa)	$6(C_{10}+C_{01})$ (MPa)	$\lim_{\lambda \to 1} \frac{d\sigma}{d\lambda}$ (MPa)	Q
Opaque	150	−0.0014	0.2920	1.7441	1.7067	0.0150
	160	−0.0057	0.2455	1.4390	1.4124	0.0403
	170	0.0007	0.1998	1.2028	1.1778	0.0680
	180	0.0073	0.1443	0.9096	0.8931	0.0417
	190	0.0086	0.1132	0.7304	0.7185	0.0273
Transparent	150	−0.0303	0.4503	2.5202	2.4650	0.0038
	160	−0.0285	0.4065	2.2679	2.2231	0.0173
	170	−0.0453	0.3596	1.8858	1.8483	0.0151
	180	−0.0452	0.2988	1.5216	1.4847	0.0077
	190	−0.0456	0.2331	1.1255	1.1006	0.0033

TABLE III Ogden material parameters for acrylic sheets (opaque and transparent) between 150 and 190°C at the crosshead speed of 250 mm/min

Type	Temperature (°C)	β (MPa)	α (MPa)	3/2 ($\alpha\beta$) (MPa)	$\lim_{\lambda\to 1}\frac{d\sigma}{d\lambda}$ (MPa)	Q
Opaque	150	2.0683	0.4311	1.3375	1.3261	0.1664
	160	1.7810	0.4000	1.0686	1.0608	0.1948
	170	1.3133	0.4690	0.9239	0.9164	0.2128
	180	0.7100	0.6590	0.7018	0.6973	0.1251
	190	0.7500	0.6000	0.6750	0.6037	0.0996
Transparent	150	128.8800	0.0100	1.9332	1.9133	0.1666
	160	90.0090	0.0191	2.5788	1.7035	0.2272
	170	85.670	0.0100	1.2851	1.2738	0.3911
	180	28.4911	0.0226	0.9658	0.9539	0.4165
	190	6.8900	0.0700	0.7235	0.7172	0.1349

TABLE IV Summary of temperature dependent critical material parametric functions of Mooney-Rivlin and Ogden models for acrylic sheets (Opaque and Transparent)

Type	Mooney-Rivlin model	R^2	Ogden model	R^2
Opaque	$C_{10} = 8\times10^{-6}\mathrm{T}^2 - 0.0024\mathrm{T} + 0.1797$	0.8164	$\alpha = 5\times10^{-5}\mathrm{T}^2 - 0.0099\mathrm{T} + 0.8332$	0.7143
	$C_{01} = 2\times10^{-5}\mathrm{T}^2 - 0.0097\mathrm{T} + 1.4111$	0.9960	$\beta = 4\times10^{-4}\mathrm{T}^2 - 0.1631\mathrm{T} + 18.268$	0.9486
	$E = 6(C_{10}+C_{01}) = 48.337\mathrm{e}^{-0.022\mathrm{T}}$	0.9939	$E = 3/2\alpha\beta = 19.026\mathrm{e}^{-0.0179\mathrm{T}}$	0.9658
Transparent	$C_{10} = 9\times10^{-6}\mathrm{T}^2 - 0.0035\mathrm{T} + 0.3011$	0.7639	$\alpha = 7\times10^{-5}\mathrm{T}^2 - 0.0226\mathrm{T} + 1.8325$	0.8835
	$C_{01} = -4\times10^{-5}\mathrm{T}^2 + 0.0086\mathrm{T} + 0.0866$	0.9998	$\beta = -0.0131\mathrm{T}^2 + 1.3893\mathrm{T} + 212.18$	0.9549
	$E = 6(C_{10}+C_{01}) = 54.697\mathrm{e}^{-0.0201\mathrm{T}}$	0.969	$E = 3/2\alpha\beta$=203.18 $\mathrm{e}^{-0.0295\mathrm{T}}$	0.8265

These material parameters vary with changing temperatures in a regular pattern. By fitting these data with either a polynomial or an exponential function, the relationship between these parameters and temperature can be formulated [1, 18]. The critical material parametric functions are listed in Table IV. Moreover, Figs 6 and 7 display the critical material parametric values, C_{10}, C_{01} in Mooney-Rivlin model and α, β in Ogden model respectively as functions of temperature. Subsequently, the initial Young's modulus E can also be derived in terms of these parameters for various material temperatures, and the relationship between the Young's modulus and temperature can be well described by the fitted exponential equations with both models, Fig. 8. The derived 2nd order polynomial and the exponential functions using both Mooney-Rivlin and Ogden models are very helpful to estimate material parameters within the testing temperature range by interpolation. However, a superior correlation is yielded from the two-term Mooney-Rivlin model compared to that from the single-term Ogden model as it is clearly shown in Tables II and III that the Q-values between experimental true stress and calculated Cauchy stress tensor in the Mooney-Rivlin model are very small (0.003–0.068) in comparison with that (0.099–0.417) in the Ogden model. In fact, Mooney-Rivlin model may be treated as a special alternative of Ogden model. As the better correlation with the experimental data can be obtained by using the higher terms of the model, it is convincing to argue that the utilisation of Mooney-Rivlin model

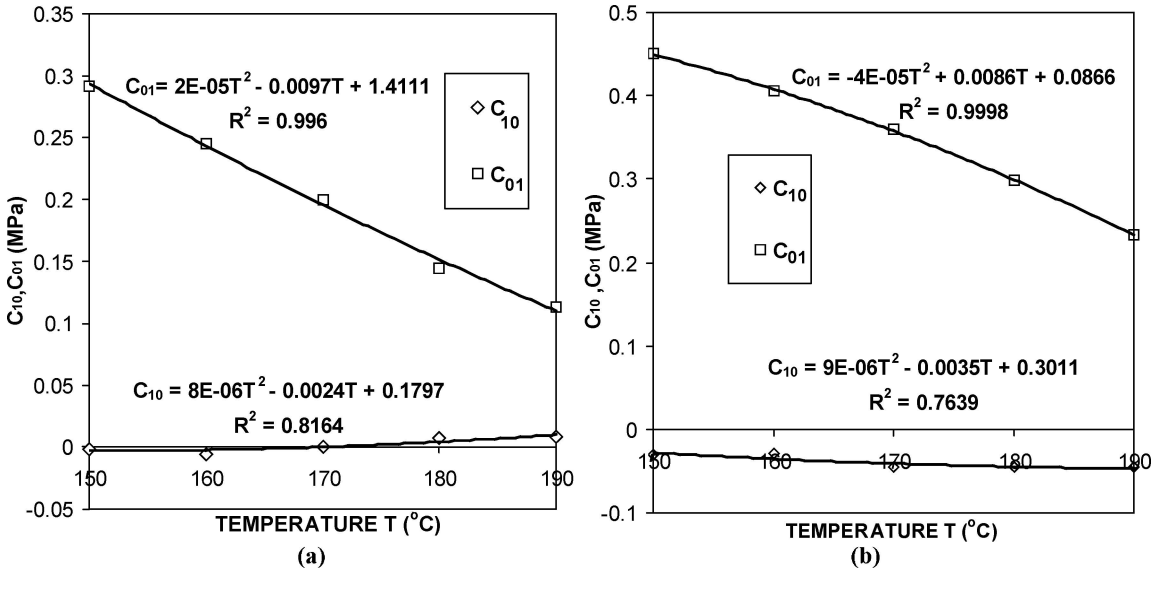

Figure 6 Material parameters C_{10} and C_{01} of Mooney-Rivlin model vs. temperature by curve fitting with the 2nd order polynomial trendlines for acrylic sheets, (a) opaque and (b) transparent.

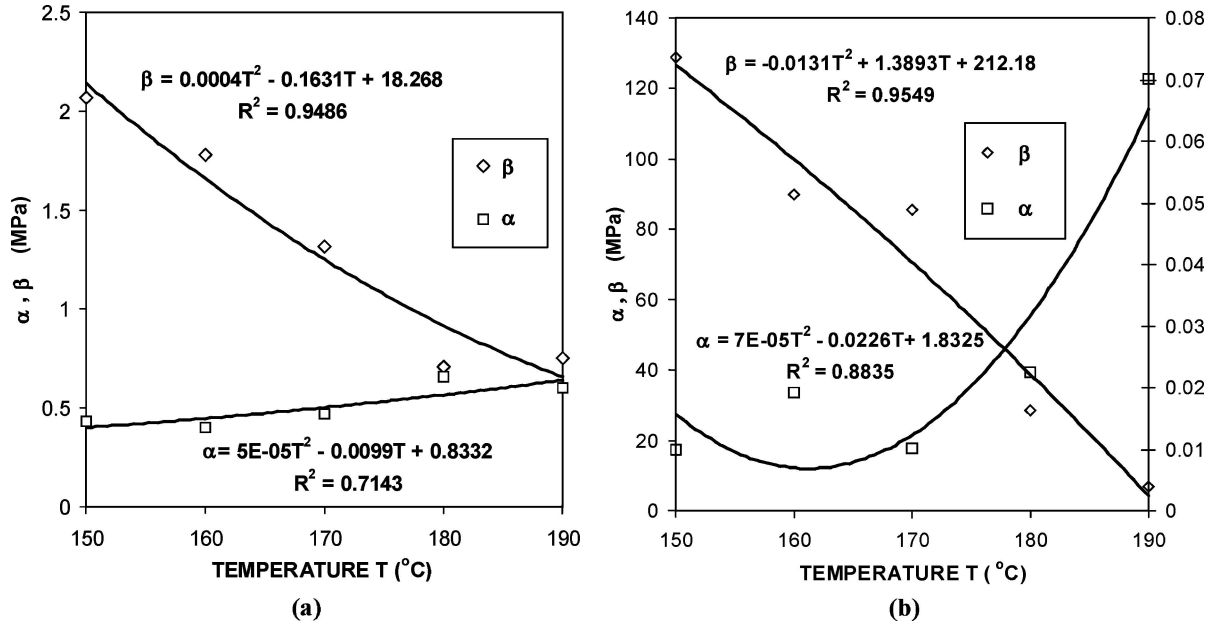

Figure 7 Material parameters α and β vs. temperature using Ogden model by curve fitting with the 2nd order polynomial trendlines for acrylic sheets, (a) opaque and (b) transparent.

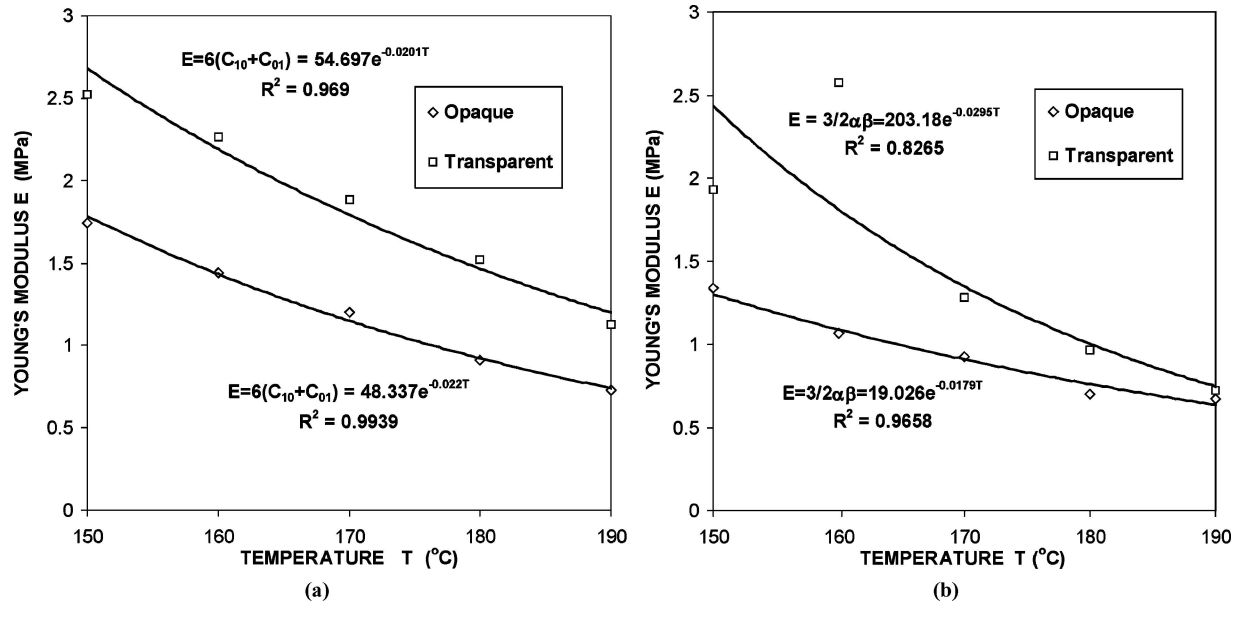

Figure 8 Young's modulus E vs. temperature using (a) Mooney-Rivlin model ($E = 6(C_{10} + C_{01})$) and (b) Ogden model ($E = 3/2\alpha\beta$) by curve fitting with exponential trendlines for opaque and transparent acrylic sheets.

will increase the accuracy of the following numerical simulation results.

4. Model validation using PAM-FORM™

In the numerical analyses of the thermoforming processes, PAM-FORM™, a centred finite differences explicit computer code, was implemented with the preparation of numerical models using pre-processor PAM-GENERIS™ and the analytical simulated results demonstrated by post-processor PAM-VIEW™ . PAM-GENERIS™ allowed the input of material property parameters, process modeling conditions and control parameters. PAM-VIEW™ is to instantaneously visualise the deformed configurations of model, and to exhibit the results such as applied load/pressure curve, thickness distribution and membrane strain. 2-D membrane elements and the conversion[1] of Mooney-Rivlin material parameters to fit Ogden constitutive law in PAM-FORM™ were used in this study.

5. Simulation of rectangular bubble inflation

The simulation of rectangular bubble inflation was also conducted with both types of acrylic sheets. Initially, the sheets (290 mm long × 100 mm wide) were meshed

[1]Ogden model in PAM-FORM™ establishes a constitutive relationship with a two-term Mooney-Rivlin model: $n = 2$, $\beta_1 = 2C_{10}$, $\alpha_1 = 2$, $\beta_2 = -2C_{01}$ and $\alpha_2 = -2$.

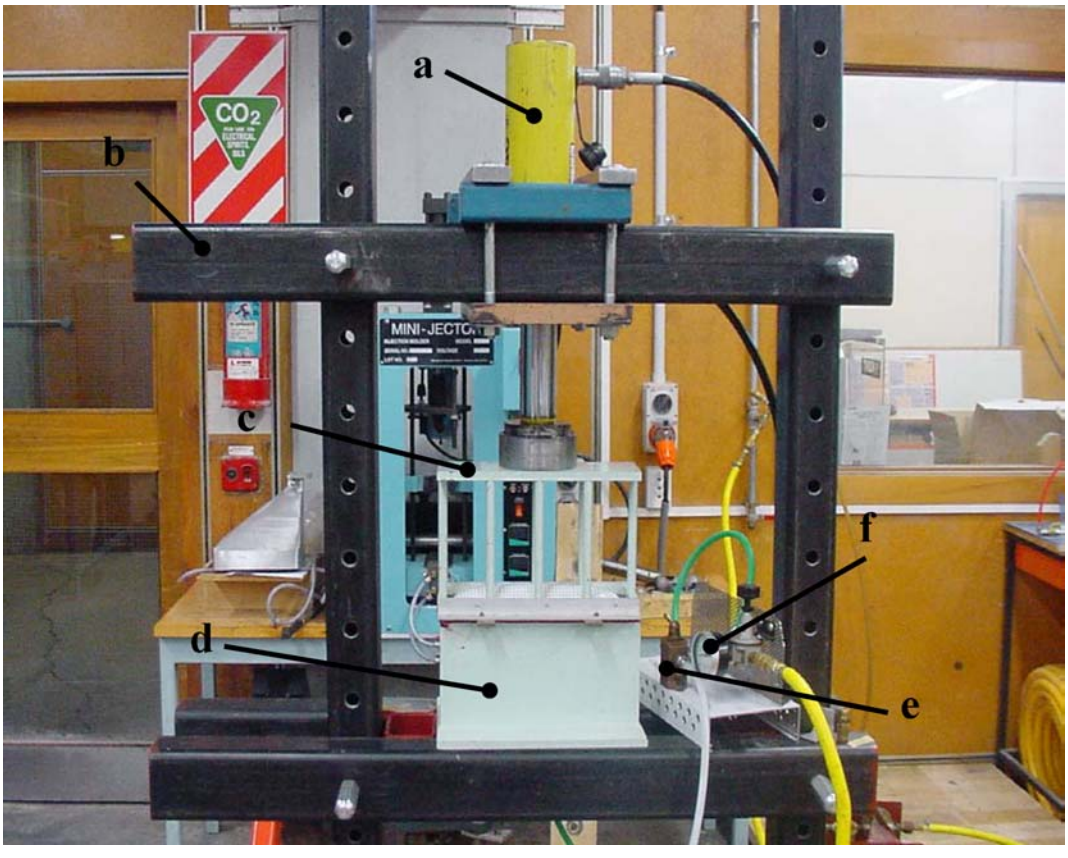

Figure 9 Apparatus of rectangular bubble inflation: (a) pneumatic press; (b) supporting frame; (c) clamping cage; (d) surge chamber; (e) air pressure valve; (f) pressure gage at the range of 0–250 kPa.

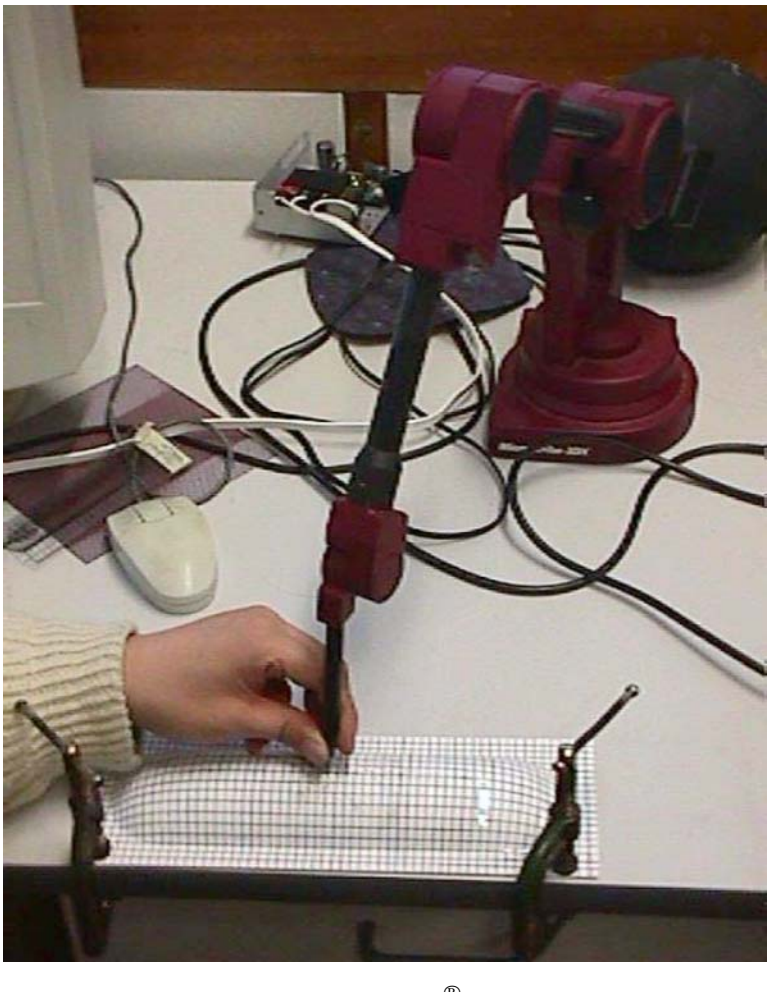

Figure 10 Spatial displacement data acquisition with Microscribe-3DX Digitiser®.

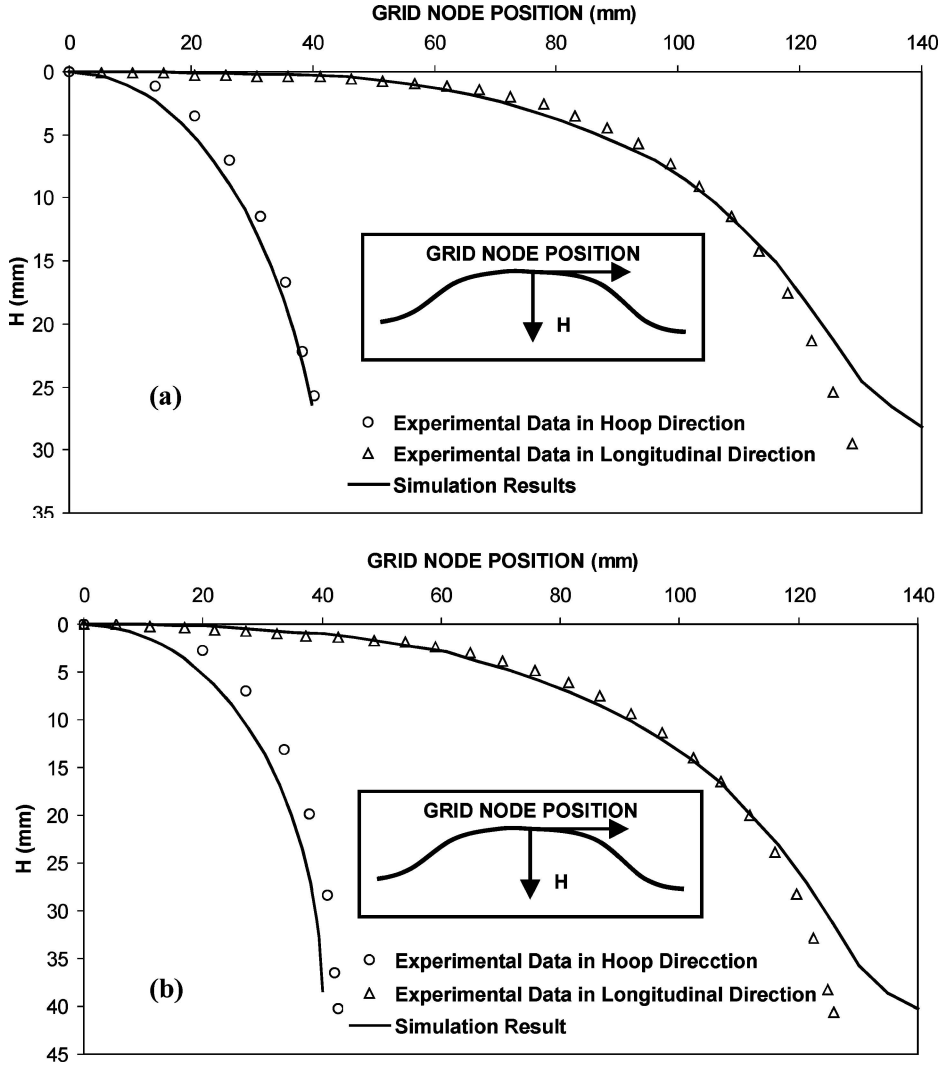

Figure 11 Profile of rectangular bubble inflation in middle portions for opaque acrylic sheet at the forming temperature 160°C, (a) differential pressure 20 kPa; (b) differential pressure 40 kPa.

with 1160 quadrilateral shell elements. Information on material parameters for the rectangular bubble inflation is illustrated in Table VI. The forming temperature was set to 160°C, which has been assumed to be uniform across the meshed sheet.

TABLE V Rectangular bubble inflation simulation: Material parameters describing Ogden model

Parameter	Temperature (°C) Uniform 160°C	Gauge differential pressure 20 kPa and 40 kPa
	Opaque type	Transparent type
Density (kg/mm^3)	1.2×10^{-6}	1.2×10^{-6}
Number of integration point	3	3
Thickness (mm)	3	2.76
Membrane hourglass coefficient	0.9	0.9
Out-of-plane hourglass coefficient	0.9	0.9
Rotational hourglass coefficient	0.9	0.9
Transverse shear correction factor	0.8333	0.8333
Ogden parameters		
α_1	2	2
α_2	−2	−2
β_1(GPa)	-1.14×10^{-5}	-5.698×10^{-5}
β_2(GPa)	-4.90×10^{-4}	-8.13×10^{-4}

The validation experiment of the bubble inflation was conducted using modified Lai's 2-D free forming apparatus [25], displayed in Fig. 9. Acrlyic sheets of the same size were prepared and marked with a 5 mm × 5 mm grid pattern. The sheets were pre-heated in the infra-red oven monitored by the 1000PID thermal controller before transferring to start the forming process at 160°C. During the inflation, based on the air flow through the pressure transducer, the differential pressure was recorded by utilising the LabView® PC data sampling system.

The experimental data, namely the distance from the apex of the bubble, were obtained along the hoop and longitudinal directions in the middle portion using a Microscribe-3DX® digitiser [26], Fig. 10. The original local Cartesian 2-D coordinates were set at grid point at the bubble apex and the corresponding coordinates of grid points along these two directions could be easily measured and converted to the relative vertical distance and grid position. Due to the symmetry of the bubble, only half grid points in the middle portions were digitised. Furthermore, the simulation results were based upon the grid node positions of inflated bubble model.

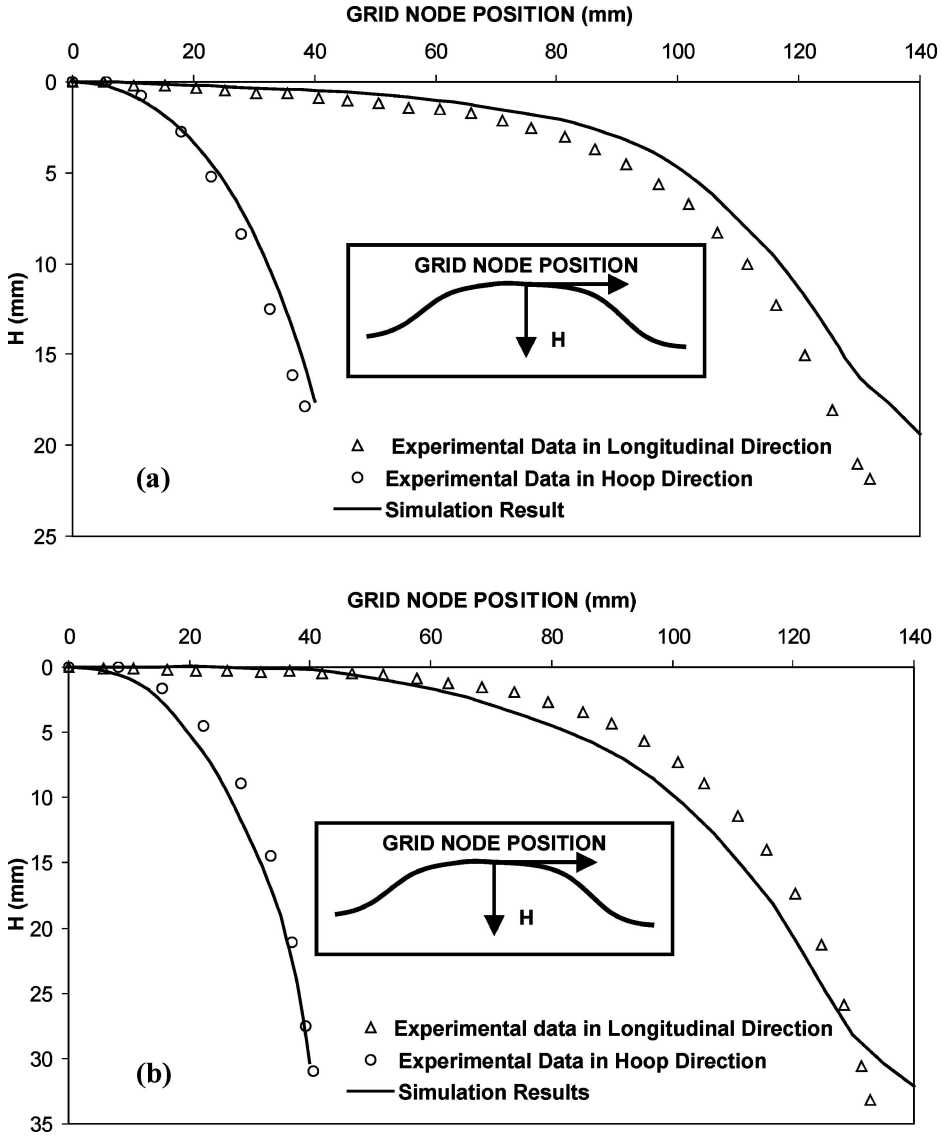

Figure 12 Profile of rectangular bubble inflation in middle portions for transparent acrylic sheet at the forming temperature 160°C, (a) differential pressure 20 kPa; (b) differential pressure 40 kPa.

The comparisons between the numerical and experimental results of bubble inflation profiles are shown in Figs 11 and 12 with the two applied gauge differential pressures of 20 and 40 kPa. Generally a good agreement of the bubble profile exists in the hoop direction although slight scattering occurs in the longitudinal direction, especially towards the longitudinal clamping region of the bubbles. This is probably due to some material flow between the clamping plates during the experiments; nevertheless in the numerical simulation it is assumed that the clamped sheet rims and the clamping plates are fully constrained [27]. The other reason might be the non-isothermal clamping edge effects because the temperature in the sheet edge is normally lower than that in the central region when the polymeric sheets are heated up in the experiments. This causes a temperature gradient from the centre of the sheet to the clamped edge whereas in the simulation, temperature is assumed to be uniform [1, 6]. The encouraging results from this initial free bubble inflation simulation warrant further investigation of components with more complex geometry, the details of which will be reported in a forthcoming paper [28].

6. Concluding remarks

This investigation has studied the material characteristics of two types of acrylic sheets under thermoforming conditions and the necessary material parameters have been identified for numerical simulation. The following concluding remarks can be made based on the observations during this study:

- From the shrinkage test, both the opaque and transparent acrylic sheets appear to show isotropic material characteristics.
- Dramatic elastic effects are demonstrated when the materials are deformed above T_g. This suggests that computer modeling on thermoforming acrylic sheets may be based on the theory of hyperelastic materials.
- The critical material parametric functions have been derived by applying least square method (LSM) to the results obtained from hot tensile tests in the thermoforming temperature range. These parametric functions, based on the prescribed Mooney-Rivlin or Ogden model, provide the basis for numerical simulation of thermoforming

processes under both isothermal and non-isothermal conditions.

- Good validation of the critical material parametric functions using simple tensile test simulation establishes the possibility of further implementations of PAMFORM^{TM} for more complex thermoforming shapes. Preliminary numerical results of bubble inflation profiles also compare well with the experimental data.

Acknowledgement

Thanks are due to Athena Products Limited, Auckland, New Zealand for supplying SHINKOLITE® acrylic sheet materials. The authors would also like to acknowledge the contributions made by Messrs Rex Halliwell and Jos Geurts, at the Strength of Materials Laboratory of the University of Auckland for assisting in the hot tensile test and bubble inflation experiments.

References

1. H. G. DELORENZI and H. F. NIED, in "Progress in Polymer Processing," edited by A. I. Isayev (Hanser, Munich, 1991) p. 117.
2. J. G. WILLIAMS, *J. Strain Anal.* **5** (1970) 49.
3. J. VLACHOPOULOS, F. A. MIRZA, B. L. KOZIEY and M. O. GHAFUR, in "Composite Sheet Forming" (Elsevier Science B.V., Amsterdam, 1997) p. 75.
4. G. MARCKMANN, E. VERRON and B. PESEUX, *Polym. Eng. Sci.* **41** (2001) 426.
5. P. BOURGIN, I. CORMEAU and T. SAINT-MATIN, *J. Mater. Proc. Tech.* **54** (1995) 1.
6. L. R SCHMIDT and J. F. Carley, *Polym. Eng. Sci.* **15** (1975) 51.
7. *Idem.*, *Int. J. Eng. Sci.* **13** (1975) 563.
8. J. MEISSNER, T. RAIBLE and S. E. STEPHENSON, *J. Rheol.* **25** (1981) 1.
9. J. MEISSNER, *J. Polym. Eng. Sci.* **27** (1987) 537.
10. L. R. G. TRELOAR, in "The Physics of Rubber Elasticity" (Oxford University Press, Oxford, UK, 1958) p. 78.
11. A. J. DEVRIES and C. BONNEBAT, *Polym. Eng. Sci.* **16** (1977) 93.
12. H. ALEXANDER, *Int. J. Engng. Sci.* **6** (1968) 549.
13. PAM-STAMP^{TM} Manuals, Pam System International (PSI), S.A. (the Software Company of ESI Group), France (2000).
14. J. BONET and R. D. WOOD, "Nonlinear Continuum Mechanics for Finite Element Analysis" (Cambridge University Press, Cambridge, UK, 1997) p. 118.
15. R. S. RIVLIN and D. W. SAUNDERS, *Phil. Trans. R. Soc.* **A 243** (1951) 251.
16. M. MOONEY, *J. Appl. Phys.* **11** (1940) 582.
17. W. W. FENG and P. HUANG, *Trans. ASME, J. Appl. Mech.* **41** (1974) 767.
18. G. J. NAM, K. H. AHN and J. W. LEE, *Polym. Eng. Sci.* **40** (2000) 2232.
19. R. W. OGDEN, *Proc. R. Soc. Lond.* **A 326** (1972) 565.
20. J. L. THRONE, "*Technology of Thermoforming*" (Hanser Publisher, Munich, 1996) p.1.
21. "Dynamic Mechanical Thermal Analyser User Guide" (Rheometric Scientific, Inc., USA, 2000).
22. H. C. LAU, S. N. BHATTACHARYA and G. J. FIELD, *Polym.Eng. Sci.* **40** (2000) 1564.
23. M. O. LAI and D. L. HOLT, *J. Appl. Polym. Sci.* **19** (1975) 1209.
24. *Idem.*, *ibid.* **19** (1975) 1805.
25. M. O. LAI, in "Thermoforming of Plastic Sheets," ME Thesis, Department of Mechanical Engineering, the University of Auckland (1974) p. 1.
26. MicroScribe 3D Users Guide, Immersion Corporation, San Jose, CA (2000). Online available: http://www.immersion.com/ digitizer/docs/microscribe3duserguide.pdf
27. G. SALA, D. L. LANDOV and D. CASSAGO, *J. Mats. Design* **23** (2002) 21.
28. Y. DONG, R. J. T. LIN and D. BHATTACHARYYA, in preparation for submission to *Polym. Eng. Sci.*

Received 14 July 2003
and accepted 31 August 2004